Available online at www.sciencedirect.com
ScienceDirect
Earth and Planetary Science Letters 255 (2007) 164–176
EPSL
www.elsevier.com/locate/epsl

Modelling carbon dioxide accumulation at Sleipner: Implications for underground carbon storage

Mike Bickle [a,*], Andy Chadwick [b], Herbert E. Huppert [c], Mark Hallworth [c], Sarah Lyle [a]

[a] Department of Earth Sciences, University of Cambridge, Downing Street, Cambridge CB2 3EQ, UK
[b] British Geological Survey, Kingsley Dunham Centre, Keyworth, Nottingham NG12 5GG, UK
[c] Institute of Theoretical Geophysics, Department of Applied Mathematics and Theoretical Physics, University of Cambridge, CMS, Wilberforce Road, Cambridge CB3 0WA, UK

Received 10 April 2006; received in revised form 23 November 2006; accepted 7 December 2006
Available online 18 January 2007
Editor: C.P. Jaupart

Abstract

An analytical solution to the equations describing the flow of a buoyant fluid released into a porous medium below a horizontal impermeable boundary is used to model the growth of CO_2 accumulations beneath thin mudstone beds in the Utsira sand reservoir at Sleipner in the North Sea. Here supercritical CO_2 has been injected at a rate of ~1 MT/yr since 1996 and imaged by time-lapse seismic data in 1999, 2001 and 2002. The CO_2 rises as a narrow plume and is partially trapped by a number of thin mudstones before reaching the caprock to the reservoir. The radii of the individual layers of trapped CO_2 increase as the square root of time since initiation as predicted by the modelling for constant input flux. However apparent negative initiation times for horizons low in the reservoir suggests that net input fluxes for these layers have decreased with time, most probably as the spreading layers have increased their leakage rates. Accumulation of CO_2 in the layers higher in the reservoir was initiated up to 3 yr after injection started. Modelling of the thickness profiles across three of the higher layers suggests that their net input fluxes have increased with time. The observation that the central thicknesses of the deeper layers have remained approximately constant, or have slightly decreased since first imaged in 1999, is consistent with the model predictions that the central thickness is directly proportional to net input flux. However, estimates of the permeability of the reservoir from the rate of increase of the radii of the CO_2 accumulations are an order of magnitude less than measured permeabilities on the reservoir sandstone. Permeabilities estimated from the modelling of layer thickness changes scatter in the same range. These discrepancies may arise from, 1) approximations in the model not being valid, 2) the measured permeabilities not being representative of the permeability for two-phase flow on the scale of the reservoir or, considered less likely, 3) that much less CO_2 is being stored in the imaged CO_2 accumulations than estimated from the seismic reflection profiles. The most probable cause of the discrepancy is that the relative permeability for the CO_2 phase is significantly reduced at lower CO_2 saturations.

Keywords: Geological carbon storage; Sleipner; Carbon dioxide; Viscous flow; Gravity flow

1. Introduction

Disposal of carbon dioxide in geological reservoirs offers perhaps the most immediate method for ameliorating anthropogenic CO_2 emissions [1]. The major

* Corresponding author. Tel.: +44 1223 333400; fax: +44 1223 333450.
E-mail address: mb72@esc.cam.ac.uk (M. Bickle).

0012-821X/$ - see front matter © 2006 Elsevier B.V. All rights reserved.
doi:10.1016/j.epsl.2006.12.013

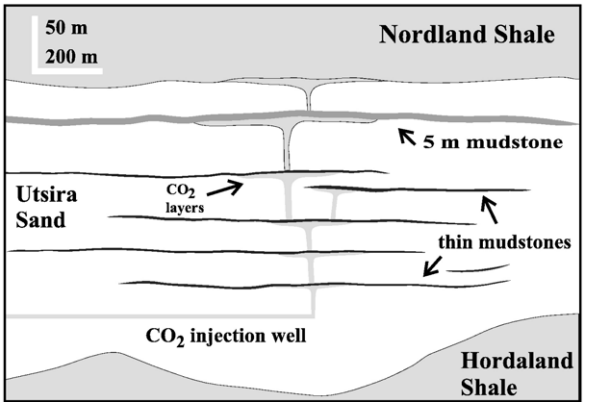

Fig. 1. Schematic illustration of CO_2 injection at Sleipner and rising CO_2 plumes being partially trapped under thin mudstones before reaching Nordland Shale cap rock. Note the vertical exaggeration.

questions about the environmental benefits of this process concern the fate of the carbon dioxide over the $\sim 10^4$ yr period required for storage [2]. Modelling the flow and retention of the carbon dioxide is beset by uncertainties. These relate to the physical structure of the reservoirs such as permeability and stratal geometries [3], problems inherent in modelling multi-phase flow [4], the behaviour of sealing strata in contact with CO_2-rich fluids [5], the possibility of reactions between CO_2 and minerals in the reservoir [6] and the rate of progressive dissolution of CO_2 in the saline fluid filling the reservoirs [7]. The information necessary for robust *a priori* predictions of these phenomena is likely to be inadequate and much of our understanding of the behaviour of CO_2 storage reservoirs will necessarily be based on observations on sites at which CO_2 is currently being injected. Most published models of the movement of CO_2 in geological reservoirs are based on numerical solutions [8,9] in which parameters are adjusted to match the known history of the reservoir before the model is used to predict future behaviour (history matching [3]). The number of poorly constrained parameters, limited data and the problems of numerical dispersion make it difficult to test the applicability of assumptions inherent in the modelling.

In this paper we model flow of CO_2 at the Sleipner storage site in the North Sea by using modifications of well known solutions for gravity flows within a permeable medium [e.g. 10] for an axisymmetric geometry [11]. This straightforward but powerful analytical approach best illustrates the controlling physics, reveals predictive aspects of the behaviour of the CO_2 and allows estimation of key reservoir parameters on the scale of the CO_2 plume.

In the Sleipner field, about 8 million tons of CO_2 have been injected since 1996 into the Utsira Sand, a $\sim$200 m thick saline aquifer. At the reservoir conditions the CO_2 is less dense than the saline fluid filling the reservoir and rises buoyantly, being partially trapped and ponded beneath a number of thin, relatively impermeable mudstone layers, before reaching the much thicker caprock overlying the Utsira Sand [12–14] (Fig. 1). Development of a prominent plume, comprising distinct layers of CO_2-saturated rock, has been tracked by time-lapse seismic surveys in 1999, 2001, 2002 [12,13]. We use the seismic images to map the increase in radius and thickness variations of the individual CO_2 layers with time [cf. 13] (Fig. 2).

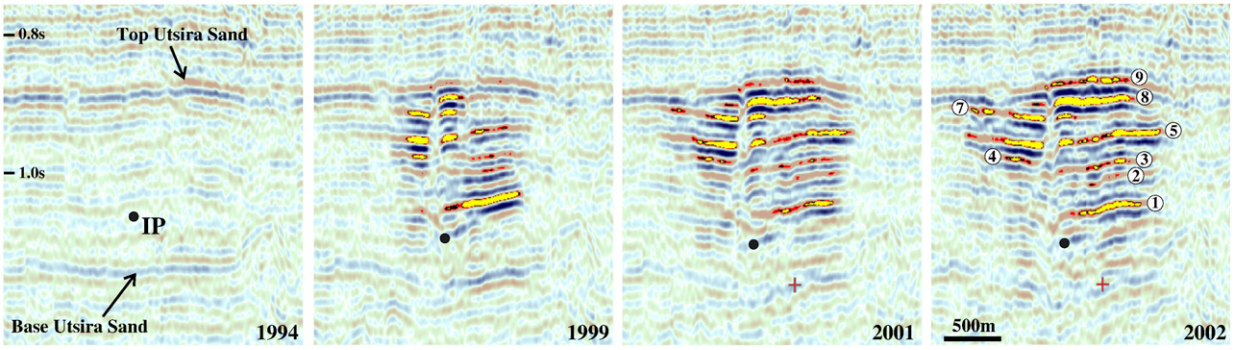

Fig. 2. Seismic reflection profiles in 1994, 1999, 2001 and 2002. The 1994 pre-injection profile shows the base and top of the Utsira Sand but little detail within the reservoir. The subsequent post-injection profiles show bright reflections where CO_2 is ponding under thin mudstones. Note the pushdown of the basal Utsira Sand reflection resulting from low velocity of CO_2 in the reservoir and development of a low amplitude vertical 'chimney' just to left (south) of the injection point (IP) presumed to be the main vertical conduit of CO_2 in the plume [15]. Layers are numbered in 2002 profile. Vertical scale is in two-way travel time.

2. Analytical solutions for axisymmetric gravity currents

Analytical solutions for gravity flows in a permeable medium with axisymmetric symmetry were presented by Lyle et al. [11], who showed that the solutions matched the results of laboratory experiments. The model is illustrated in Fig. 3 and comprises a permeable medium filled with a fluid into which a less dense and more viscous fluid is introduced along a vertical line source under a flat impermeable cap. The fluid ponds under the cap and spreads with axisymmetric symmetry. Neglecting the motion of the fluid initially saturating the porous medium (i.e. assuming its viscosity is not large compared to that of the introduced fluid), neglecting capillary forces, and solving Darcy's Law and the continuity equation gives key relationships between the rate of fluid introduction, $\alpha Q t^{\alpha-1}$, the radius of the ponding fluid, $r_N(t)$, as a function of time, t and the thickness, h, of the ponded fluid as a function of position, r and time, t. The function, $\alpha Q t^{\alpha-1}$, describes the net input flux (net input flux is presumed to equal the flux from below less any leakage through the caprock seal) and corresponds to an instantaneous release of fluid if $\alpha=0$ and a release at constant flux, Q, for $\alpha=1$. The radius is given by Eq. (2.10) in [11], except that the left hand side of Eq. (2.7) in [11] is incorrect and should be multiplied by ϕ and Q divided by ϕ in all the following equations in [11]) so that

$$r_N(t) = \eta_N(\alpha)(\gamma Q/\phi)^{\frac{1}{4}} t^{(\alpha+1)/4}, \tag{1}$$

where

$$\gamma = \rho k g'/(\phi\mu). \tag{2}$$

ρ is the density of the introduced fluid, k is permeability, ϕ porosity, μ viscosity, and $g'=g\Delta\rho/\rho$, the reduced gravity (relative density) with g the gravitational constant and $\Delta\rho$ the difference in density between the introduced fluid and the initial fluid filling the reservoir. The similarity variable, η, is given by (Eq. (2.9) [11])

$$\eta = (\gamma Q/\phi)^{-\frac{1}{4}} r t^{-(\alpha+1)/4} \tag{3}$$

$\eta_N(\alpha)$ (i.e. η at $r=r_N$) is a function of α only and is given by (Eq. (2.14) [11])

$$\eta_N = \left[2\pi \int_0^1 y f(y) \mathrm{d}y\right]^{-1/4}, \tag{4}$$

where the scaled similarity variable, $y=\eta/\eta_N$, varies from 0 at the source to 1 at the limit of the CO_2 pool and $f(y)$ is given by numerical solution of the differential equation (Eq. (2.12) [11])

$$\frac{\mathrm{d}}{\mathrm{d}y}\left(yf\frac{\partial f}{\partial y}\right) + \frac{1}{4}(1+\alpha)y^2\frac{\partial f}{\partial y} + \frac{1}{2}(1-\alpha)yf = 0, \tag{5}$$

given

$$f = \frac{1}{4}(1+\alpha)(1-y)(y\rightarrow 1). \tag{6}$$

Eq. (6) is a good approximation for f except when y is small, and η_N is well approximated by

$$\eta_N = [12/\pi(1+\alpha)]^{\frac{1}{4}}. \tag{7}$$

The thickness, h, of the flow is given by (Eq. (2.11) [11])

$$h(r,t) = \eta_N^2 (Q/(\phi\gamma))^{1/2} t^{(\alpha-1)/2} f(y). \tag{8}$$

These equations predict that at constant input flux ($\alpha=1$), 1) the radius of the CO_2 pools will be proportional to the square root of time; 2) the thickness close to the centre of the pool, $h(0,t)$, is nearly invariant; and 3) there are simple relationships between both the radius and thickness of the CO_2 pools and the input flux and physical parameters porosity, viscosity and permeability. In the next section we explore the extent to which these relationships can be used to investigate the properties and behaviour of the reservoir.

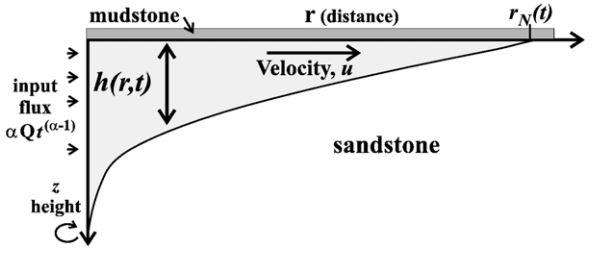

Fig. 3. Model for gravity driven flow of a less dense viscous fluid introduced along axis at $r=0$ into a porous medium initially filled with fluid of higher density. Note that only the density differences and the horizontal motions are taken into account and that viscous flow in the fluid initially filling the sandstone is ignored.

3. Seismic imaging of the Sleipner reservoir

3.1. Plume reflectivity

A baseline 3D seismic survey covering an area of 24 km by 30 km was carried out in 1994. Injection started in October 1996, and three repeat surveys, covering ~21 km^2 above the injection point, were carried

out in October 1999, September 2001 and July 2002. The baseline survey shows reflections from the top and base of the Utsira Sand but the internal reservoir structure is largely unresolved (Fig. 2, [13]). The 1999 and subsequent surveys image the CO_2 plume as a number of prominent bright reflections, with nine or more distinct seismic layers [12]. A vertical zone of reduced reflectivity and enhanced velocity pushdown lies roughly above the injection point, and is interpreted as a vertical 'chimney' of CO_2 which forms the main conduit of CO_2 upwards through the reservoir [13]. The bright reflections mostly correspond to reflection doublets, interpreted as interference wavelets from thin (a few metres thick) layers of CO_2 saturated sand. (Fig. 2, [12]). The topmost CO_2 layer directly underlies the Nordland Shale which forms the upper seal to the Utsira reservoir. The lower layers are thought to be accumulating beneath ~ 1 m thick mudstone layers picked out as spikes on geophysical well logs [14]. It is emphasised however that no well penetrates the plume itself, so that the exact number and structural disposition of intra-reservoir mudstones within the plume envelope is not known.

Relative amplitude maps of the reflections in 1999, 2001 and 2002 (Fig. 4, e.g. [15]) show them to be roughly circular to ellipsoidal in plan, growing with time and having the highest amplitudes in their centres. The waveforms of the reflections from the CO_2 layers are characteristic of thin layer interference, consistent with thicknesses beneath the limit of seismic resolution ($\lambda/4$ or around 8 m). In this situation amplitude varies directly with layer thickness. The variations in thickness of the CO_2 layers may be estimated directly from the variations in amplitude by assuming that the maximum observed amplitude in each CO_2 layer corresponds to the tuning thickness of ~8 m [15]. Lyle [17] showed that the amplitude of the interference doublet also depends on the thickness of the overlying mudstone with each metre increase in mudstone thickness raising the reflection amplitude by about 3%. Thus Layer 8 has reflection amplitudes that are systematically some 20% higher than those of the other layers. This is consistent with wireline logs which show that the mudstone overlying Layer 8 may be 5 m or more thick [14] compared with the ~1 m thickness of the mudstones overlying other layers. Estimated CO_2 layer thicknesses therefore incorporate uncertainties arising from the assumed maximum tuning amplitude and also mudstone thickness.

The total volume of CO_2 in the reservoir was estimated from reflection amplitudes and the velocity pushdown by Chadwick et al. [15] who suggested that around 85% of the CO_2 plume in 1999 could be accounted for in the reflective layers, with the rest distributed in a dispersed low saturation form in between the layers or dissolved within the saline reservoir fluid.

A major uncertainty in the calculations of CO_2 volumes is the reservoir temperature, which strongly influences the physical properties of CO_2. A single reservoir measurement indicates a temperature at the injection point of about 36 °C, but regional geothermal studies suggest that the temperature at the injection point is 41 ± 1 °C (Statoil personal communication). Other significant uncertainties include the thickness-amplitude calibration of the layer reflections, the fine-scale nature of the dispersed CO_2 that influences the seismic velocity response and CO_2 saturations within the layers (dependent on capillary forces which determine how much CO_2 can replace the formation water).

A number of possible geological controls on the lateral spreading of the CO_2 layers are evident (Fig. 4). These include: 1) sharply defined and nearly static layer boundaries, with Layers 1 and 2 bounded to the west and Layers 4, 5 and 9 bounded to the south-east; 2) various linear features such as a NW–SE trending structure on Layer 5 and the prominent northward prolongation on Layer 9; and 3) a tendency in some of the layers towards elliptical morphology in plan view. The static layer edges are suggestive of lateral permeability barriers or steeper seal topography, the linear features may relate to faults or sedimentary channels with permeabilities different to surrounding strata, and the prominent tongue on Layer 9 corresponds to a ridge-like topographic high in the overlying caprock. Elliptical layer morphologies may reflect either layer seal topography or anisotropic reservoir permeability. Vella and Huppert [16] show that gravity currents accumulating under a sloping barrier will tend to flow predominantly upslope after a critical time which depends on the slope, injection rate and reservoir parameters. For a 1° slope and the range of parameters appropriate for the Sleipner field, they estimate such times as between 0.03 and 14 yr. The Sleipner CO_2 layers vary from near circular (layers 6 and 8) to elliptical with aspect ratios approaching 3 (layer 5). The cause and consequences of such asymmetry are clearly important for modelling the fate of the CO_2. In this work we treat the accumulations as axisymmetric as discussed below. There is a general increase in reflection amplitudes (and implied thicknesses) towards the centre of the layers, although many of the layers show distinct, localised, areas of high amplitude that are consistent across two or more repeat surveys. These may reflect topographic highs in the layer seals, underlain by thicker ponded CO_2 [13,15]. Other complexities include the possibility that some

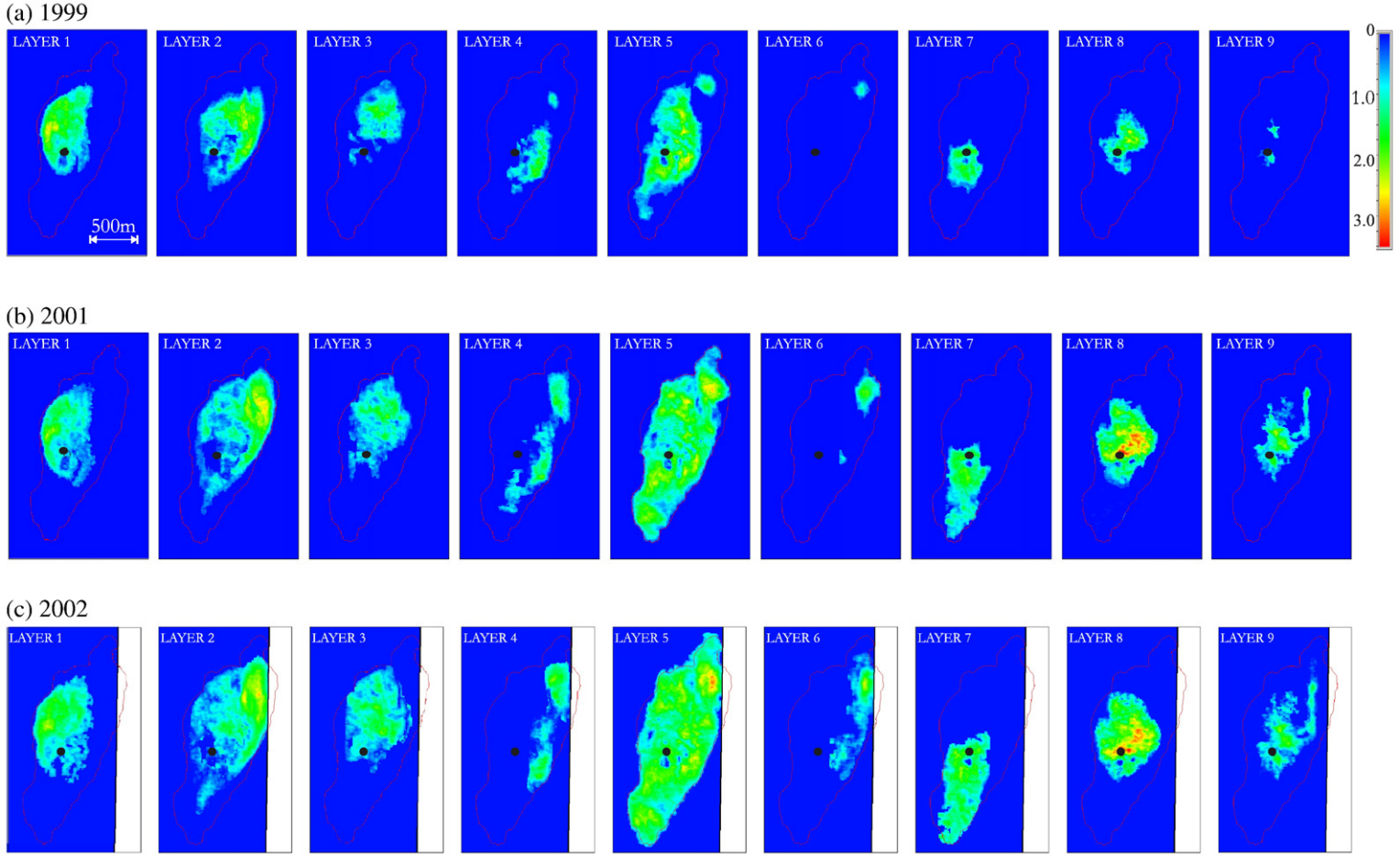

Fig. 4. Maps showing the relative seismic amplitude of the bright reflections on the 1999, 2001 and 2002 seismic surveys. These correspond to the tops of the CO_2-saturated layers. Black spot corresponds to injection point. Red polygon denotes full areal extent of 2002 plume.

layers seem to spread from more than one centre (e.g. Layers 4 and 8), parts of layers grow dimmer with time (e.g. Layers 1 and 2) and some layers were initiated significantly later than the 1996 start of injection (discussed in detail below).

3.2. Layer growth

Changes with time in layer growth and reflectivity provide qualitative insights into plume dynamics. All of the layers developed progressively from 1999 to 2002, but the nature of this development changes significantly from the base of the plume to the top (Fig. 4). The lower layers, exemplified by Layer 1, showed relatively modest lateral spreading from 1999 to 2002. Reflectivity increases were largely restricted to the outermost parts of the layers, associated with layer spreading. Axial parts of the lower layers showed more stable reflection amplitudes, with a tendency towards reduced reflectivity. In the upper plume, the layers grew much more rapidly. Increased reflectivity at layer edges corresponded to layer spreading and thickening. Reflectivity also increased markedly in the axial parts of the layers between 1999 and 2001, but less so from 2001 to 2002, consistent with a progressive stabilisation of axial thicknesses.

Thicknesses in the central parts of layers seem to have stabilised; indeed, decreased reflection amplitudes with time in lower layers may even suggest layer thinning. This latter interpretation must be treated with considerable caution however, as a number of purely seismic related factors are likely to progressively attenuate seismic signal in the lower plume as amounts of CO_2 increase. In the upper plume, layers show continued growth. From 1999 to 2001 this involved both thickening and layer spreading, whereas from 200l to 2002 lateral spreading became the dominant growth process.

4. Modelling growth of the CO_2 accumulations

4.1. Radial growth rate and initiation time

Layer growth was examined by measuring the plan area of each layer (Fig. 4) and calculating the radius of a circular layer with an equivalent area. Fig. 5 plots the radius squared for each CO_2 layer against time with estimated upper and lower bounds as indicated. The least-squares linear fits are also shown with the 1σ uncertainty on each estimate of the square of radius calculated by assuming that the difference between the upper and lower bounds represents $\pm 2\sigma$. From 1999 onwards, the increase in mean radius is within error of being proportional to the square root of time for all the layers, as predicted by Eq. (1) for $\alpha = 1$ (constant net flux). As discussed further below, because the 2001 and 2001 seismic surveys are very close in time, the data admit a relatively large uncertainty on α. Several of the lower layers (1, 2, 3 and 4S) have negative time intercepts at zero radius indicating deviations from the linear fits prior to 1999, most probably because net input fluxes decrease (net input flux is defined as the input flux less any leakage through the mudstone seal). The other layers exhibit significant delays between the start of injection in 1996 and start of accumulation at the horizon. These range up to nearly 3 yr for Layers 4N and 9. As discussed below, the variation in thickness with time of some of these layers is best modelled with net input fluxes increasing with time but the lack of early seismic surveys admits considerable uncertainty on the estimates of initiation times. In general, initiation times become later higher in the reservoir (Fig. 6). This is consistent with the CO_2 initially ponding below lower mudstone seals and then progressively leaking through the seals to penetrate higher in the reservoir.

4.2. Quantification of CO_2 volumes and permeabilities from radii estimates

There is considerable interest in quantifying the volume of CO_2 stored in the reservoir and modelling flows of CO_2 within the reservoir. Many of the reservoir parameters needed to do this are relatively well constrained (Table 1). The exceptions are reservoir temperature, to which both CO_2 viscosity and density are sensitive, and permeability, for which measured values range over a factor of three or more. These parameters are all incorporated in the single parameter, γ (Eq. (2)), which controls the shape of the CO_2 layers. In general, the estimates of the radial extent of the CO_2 layers are thought to be more robust than estimates of their thickness, because of uncertainties in the calibration of thickness, the effects of seal topography and attenuation of the seismic signal by passage through the overlying CO_2 layers. We have therefore taken two simple approaches to analyse the data. The first is to calculate a best estimate for the constant γ from the radial growth rate estimates with the assumption that all the CO_2 injected is stored in the observed layers. The second is to constrain the volume of CO_2 (Qt^{α}), parameter γ, initiation time t_0, and variations in input flux described by α, by modelling the evolution of individual layers for which we think the estimates of thickness as a function of radius are most reliable.

Table 2 summarises calculated temperatures, pressures, input fluxes and cumulative CO_2 mass for the

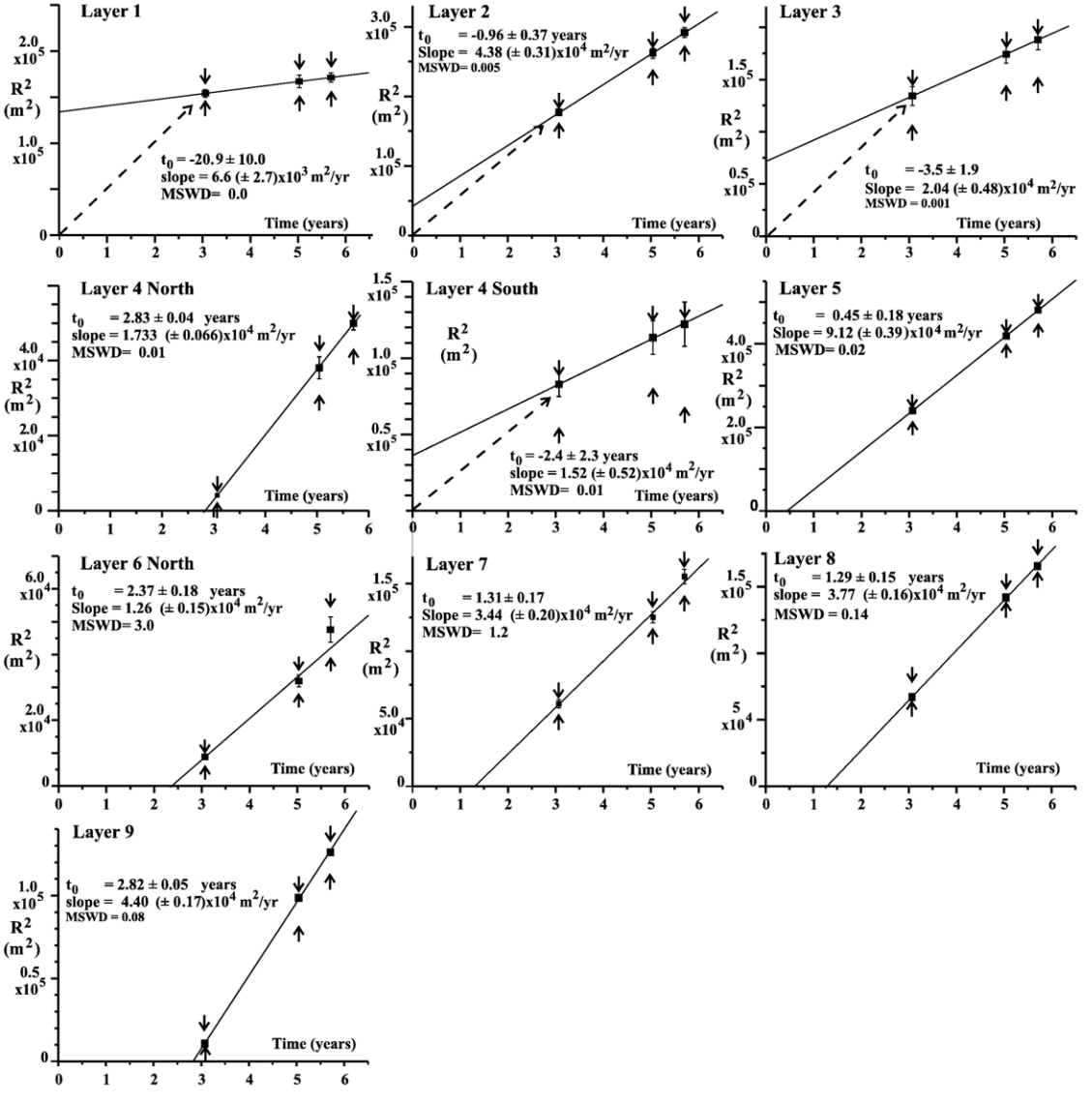

Fig. 5. Square of radii (m^2) calculated from measured areas plotted against time (years since injection initiated) for CO_2 accumulations. Dashed lines show possible growth curves for accumulations which exhibit decreases in growth rates. Arrows show estimated maximum and minimum limit on radii. Least-squares best fit regressions of time against radius squared after [18], with inferred time each accumulation initiated (t_0) and slope with 1σ uncertainties and mean squared weighted deviate (MSWD) shown on each plot.

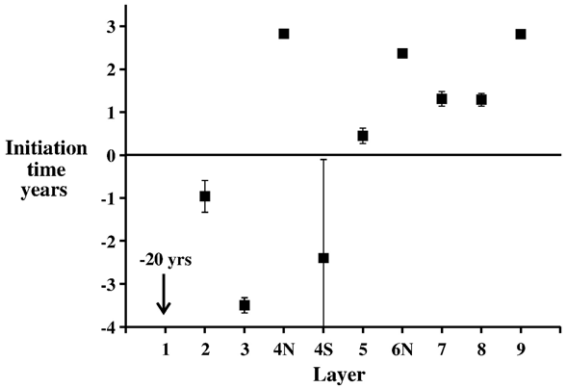

Fig. 6. Apparent initiation times for individual accumulations calculated from intercepts on the plots of radius squared versus time (Fig. 5). Note deeper layers must exhibit decreasing growth rates presumed to result from reduced supply or increased leakage with time, whereas higher layers initiate later and/or had CO_2 supply increasing with time. Error bars reflect the 1σ uncertainty from the least-squares fits in Fig. 5 and do not include that arising from the assumption that $\alpha = 1$.

nine layers identified by the seismic surveys calculated from least-squares fits in Fig. 5 assuming that all the injected CO_2 is stored in the layers imaged and the temperature at the injection point is 41 °C. Layer 4 is considered as two separate accumulations (north and south) fed by two separate supplies. Layer 9 is modelled as one accumulation although, as discussed below, it may have grown from two sources and amalgamated. The input fluxes and amount of CO_2 stored for each layer are calculated from the slopes of the radius-squared data and the initiation times given in Fig. 5 for the parameters in Table 1 using Eq. (1). Because the density and viscosity of CO_2 vary rapidly with temperature and pressure, these have been calculated separately for each layer. The remaining parameters in γ (kg/ϕ) have then been adjusted so that the estimated mass of stored CO_2 in 2002 is equal to the mass injected by that time (4.92 MT), less 40% to allow for the likely underestimate in radius from the seismic amplitude maps as discussed below. Given the values of parameters in Table 1, the calculated permeability is $0.187 \pm 0.014 \times 10^{-12}$ m^2 (2σ), assuming the temperature at the injection point is 41 °C. The negative initiation times for Layers 1, 2, 3 and 4S (Fig. 6) have been retained in the calculations because this is necessary for description of the layer geometry from which the volumes are calculated. This is equivalent to assuming that the layers adjust their shapes rapidly after the inferred pre-1999 decrease in net input flux to that appropriate to the reduced input flux. The uncertainties in the calculated durations, input fluxes and CO_2 accumulated are propagated from the uncertainties in the growth rate fits shown in Fig. 5 taking into account the covariances.

4.3. Modelling of layer thickness profiles

Where the data appears to be reliable and layer growth is thought to approximate an axisymmetric accumulation, it is also possible to examine model fits to the thickness profiles directly. Layer 6N exhibits little evidence of topographic control and is situated away from the main plume and consequently suffers little from signal attenuation by overlying layers. Layer 8 is approximately circular, shows consistent growth and is near the top of the plume which reduces signal attenuation by overlying layers. Layer 9 shows two accumulations developing in 1999 with strong topographic control on the northern part (Fig. 4). By 2001 these accumulations have amalgamated but the seismic amplitude map and thickness profiles suggest that the northern and southern accumulations are growing from separate supplies or the northern accumulation is fed horizontally from the southern part. The southern accumulation is modelled because this exhibits the least obvious topographic control. Fig. 7 shows thickness profiles for layers 6N, 8 and 9S estimated from the 2002 seismic surveys. Radii measured from the position of maximum thickness differ by up to a factor of two. The asymmetry may arise because of sloping

Table 1
Reservoir parameters

CO_2 density[1] (kg/m^3)	Saline fluid density[1] (kg/m^3)	1 sigma	CO_2 viscosity[1] (Pa s)	1 sigma	Effective porosity[2]	1 sigma	Permeability[3] (m^2)	T[4] (°C)	Pressure[5] (MPa)
~420–610	1020	20	$3.0–5.0 \times 10^{-5}$	$\sim 4 \times 10^{-6}$	0.300	0.030	1.1 to 5×10^{-12}	35–40	8.0–10.0

1: using routines in TOUGH2 [19], 2: after [20] but adjusted for a nominal CO_2 saturation of ~0.8, 3: two measurements on core gave 2.5 and 3.3×10^{-12} m^2, and well test data on Utsira Sand in the Grane and Osberg fields gave 5.8 and between 1.10 to 8.14×10^{-12} m^2. 4: The best estimate of the temperature at the injection depth (1012 m bsl) is 41 ± 1 °C (Statoil personal communication 2005) and temperatures at layers are calculated from this temperature, a seabed temperature of 7 °C at 80 m bsl and thermal conductivity (K, W $m^{-1}.°C^{-1}$) varying with depth as $1/K = 0.80–2.2E{-}4 * d - 2.4E{-}8 * d^2$ ($d < 720$ m) and $1/K = 0.62–6.0E{-}5 * d - 6.6E{-}8 * d^2$ ($d > 720$ m) where d is depth below seabed (m). 5: calculated assuming pressures are hydrostatic.

Table 2
CO_2 accumulation parameters

Layer	P (MPa)	T (°C)	Density (kg/m^3)	Viscosity (Pa s)	Flux (MT/yr)	1 sigma	Integrated mass (MT)	1 sigma
1	9.7	39.8	607	4.56E−05	2.51E−03	2.03E−03	0.066	0.028
2	9.3	38.6	591	4.40E−05	1.01E−01	1.46E−02	0.674	0.061
3	9.1	38.1	586	4.34E−05	2.13E−02	9.92E−03	0.196	0.052
4N	9.0	37.7	577	4.26E−05	1.45E−02	1.10E−03	0.042	0.003
4S	9.0	37.7	577	4.26E−05	1.12E−02	7.70E−03	0.090	0.038
5	8.8	37.1	564	4.14E−05	3.72E−01	3.16E−02	1.952	0.103
6N	8.6	36.6	544	3.97E−05	6.43E−03	8.65E−04	0.021	0.002
7	8.4	36.1	530	3.84E−05	4.29E−02	4.87E−03	0.189	0.015
8	8.2	35.5	490	3.52E−05	4.04E−02	3.39E−03	0.178	0.009
9	8.0	35.0	426	3.03E−05	3.67E−02	2.91E−03	0.106	0.007
						Total	3.51	0.14

caprock [16], anisotropic permeabilities or even flow of the saline brine within the reservoir.

Radial distances in Fig. 8 have been normalised to the root-mean squared radius by the following procedure. The magnitude of the four principle radii for each horizon are estimated by taking the zero intercept of a least-squares fit of thickness against radius measured from the position with maximum thickness. The radial distances have then been normalised by a linear proportional transformation to the root-mean radius. The 2002 values of r_N for Layers 6N and 8 calculated from the least-squares fits in Fig. 7 are ~25% and 8% greater than estimates calculated from the measured areas. This is because seismic amplitudes are below the detection limit for CO_2 thicknesses of less than ~0.5 m and the slope of the CO_2 layer surface is shallow near the margin. The difference is significant to calculation of the volume of CO_2 stored from the area measurements because the input flux, Q, scales as r_N^4 (Eq. (1)) resulting in a ~40% underestimate of the stored volume calculated from the areas, for a 15% underestimate of the radius.

All three layers show an increase in central thickness with time (Fig. 8). If the CO_2 input flux is constant, that is $\alpha=1$, Eq. (8) implies that layers grow by simple stretching of the profile such that the central thickness changes little. Central thickness reflects the net CO_2 input flux and it is of interest to examine constraints available on changes in this parameter. By contrast Layers 1, 2, 3 and 5 show either little change in central thickness or even a slight decrease (Layers 1 and 2), indicative of constant or decreasing net input fluxes after 1999. This is consistent with the decrease in net flux into these layers implied by the apparent negative initiation times.

The variation of thickness with time and radial distance is a function of three parameters in Eq. (8): Q, α and γ. The time at which horizon growth is initiated (t_0), and the constants Q (m^3 s$^{1/\alpha}$) and α in the expression describing the input flux are the main unknowns describing the flow of CO_2, presuming that varying fluxes may be approximated by the mathematically convenient term $\alpha Q t^{(\alpha-1)}$. γ is a function of the reservoir

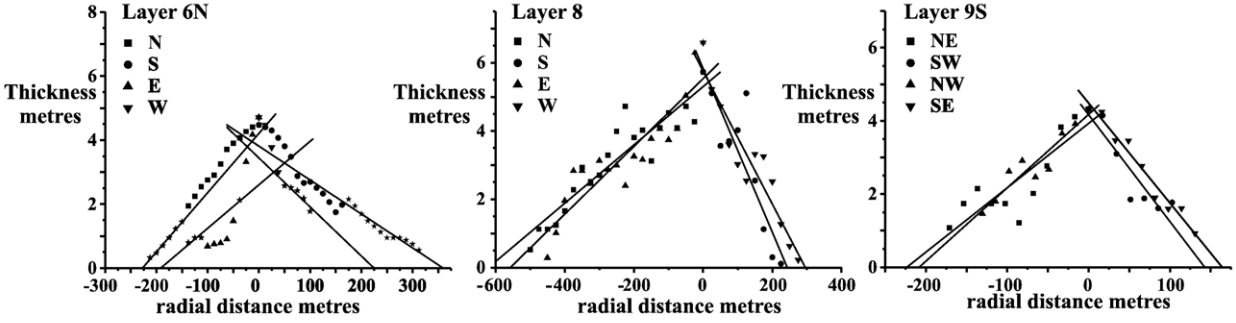

Fig. 7. Thickness of layers 6N, 8 and 9S calculated from 2002 seismic survey plotted against radius for two orthogonal profiles. Lines are least squares fits used to calculate the magnitude of the local radius of each CO_2 accumulation which are then used to normalise radial distances (see text). The stars in plot of layer 6N are points used in regression.

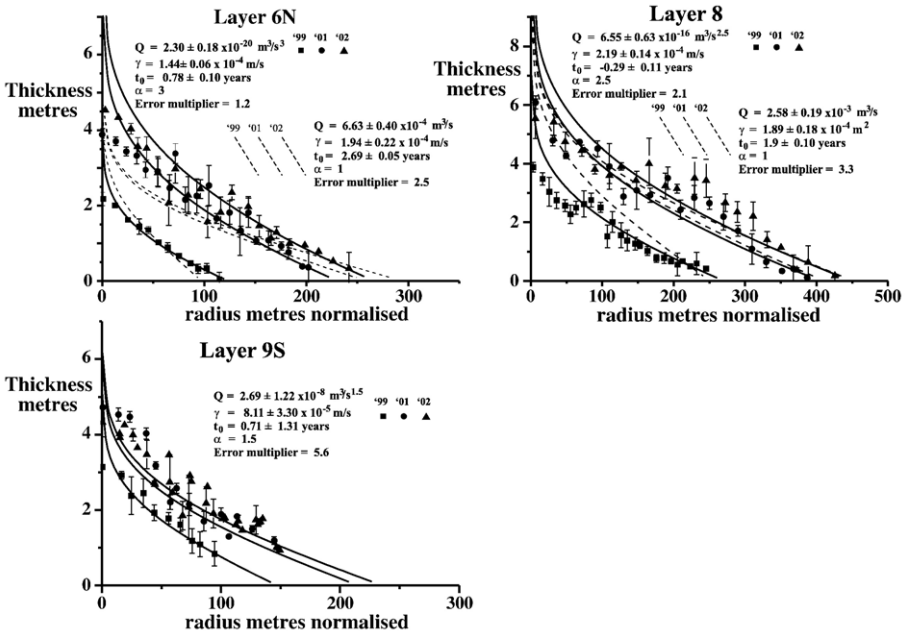

Fig. 8. Data and the corresponding least squares fits with the data binned in 10 m intervals of radius (Layers 6N and 9S) or 20 m intervals (Layer 8). Error bars are ±1 standard error on mean thickness in the bin. Curves are least-squares fits to Eq. (8) for parameters in Table 1, α as given and constant Q in input flux, $\alpha Q t^{(\alpha-1)}$, constant γ (Eq. (2)), and initiation time, t_0, as adjustable parameters. Best fit values of these parameters are shown on figure with 1σ uncertainties. The error multiplier is the factor by which the uncertainties, estimated from the standard errors on the binned data, need to be increased to give a fit with the χ^2 predicted for the degrees of freedom. Layer 6 gives the best fits with $\alpha \geq 2.5$ but t_0 is negative for $\alpha > 3.5$. Solutions for Layer 8 with higher values of α give better fits except that the initiation times become negative if $\alpha > 2.5$. Fits to Layer 9S give negative t_0 for $\alpha > 1.5$. Fits with $\alpha = 1$ are shown as dashed lines and do not model the increasing central thickness of any of the layers. Thicknesses estimates (open symbols) at radii less than $\sim 0.2 \times r_N$ have been excluded from the fits because the model vertical line source input is not appropriate for input over a finite area [11].

parameters listed in Table 1 which are mostly known to within ±10% at given temperature and pressure. However measurements of the permeability are more problematic as discussed above. The ranges of the parameters t_0, Q, α, and γ which best describe Layers 6N, 8 and 9S have been investigated by least-squares minimisation of scatter in thicknesses about the model fits against radius. Although radius-thickness plots are available for 1999, 2001 and 2002, the latter are too closely spaced to provide more than one effective constraint. Therefore estimates of t_0, Q and α have significant correlated uncertainties. The permeability controls the shape in that higher values of γ result in a larger radius but thinner accumulations. Illustrative least-squares fits are shown in Fig. 8.

Layer 6 gives fits with scatter close to that estimated from the standard error of the 10 m bins of radius with $\alpha \geq 2.5$. The fits on Layer 8 improve as α increases but the initiation time becomes negative for $\alpha > 2.5$. Layer 9S data is more scattered with no significant statistical difference between fits with $\alpha \geq 1$. Fig. 9 shows the radius squared versus time fits for the values of alpha illustrated and the values of r_N estimated from the fits versus those derived from measured layer areas.

4.4. Comparison of model and measured permeabilities

The values of γ estimated from the least-squares fits to the thickness-radius data are very insensitive to the choice of α with a range of 1.44 to 1.45×10^{-4} m/s (1σ) for Layer 6N ($2.0 \leq \alpha \leq 3.5$), 2.08 to 2.19×10^{-4} m/s ($1.5 \leq \alpha \leq 2.5$) for Layer 8, and 7.8 to 8.2×10^{-5} m/s for Layer 9S ($1.0 \leq \alpha \leq 2.0$). The statistical uncertainty arising from the least squares fitting dominates the uncertainties (Fig. 8). The values of permeability derived from the layer thickness profiles are illustrated as a function of temperature at the injection point in Fig. 10 and compared with the estimates from the whole-reservoir modelling. Layers 6N and 8 imply permeabilities of $\sim 0.4 \times 10^{-12}$ m^2, Layer 9S, $\sim 0.1 \times 10^{-12}$ m^2 and the whole-reservoir model 0.19×10^{-12} m^2. Only for Layer 8, with the temperature at the injection point significantly lower than the best estimate (that is < 37 °C), do any of the calculated permeabilities approach the

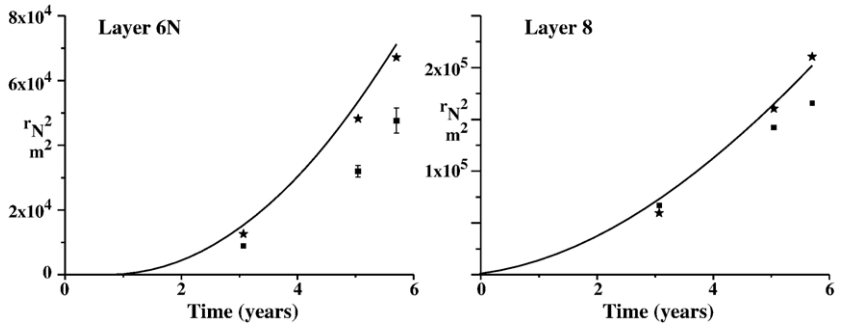

Fig. 9. Least-squares fits of radius-squared versus time comparing 1) radius calculated from measured areas (squares), 2) radius calculated as root mean of estimates from thickness profiles (stars) and 3) radii computed from best fits to normalised radial distances as shown in Fig. 8 (line).

measured values. The permeabilities estimated from the whole-reservoir model vary more rapidly with temperature than those estimated from modelling the layer thicknesses. This is because in the whole-reservoir model a density term occurs both in the conversion from mass-input to volume and in the parameter γ which determines the ratio of layer thickness to radius.

A number of factors could cause the apparent discrepancy between estimated and measured permeabilities, including 1) that the CO_2 layers pond buoyantly beneath topographic highs, thereby increasing their thickness to radius ratios (the reservoir was deliberately sited under a small structural dome); 2) permeability measurements on individual ~cm sized core samples and the drill bore tests are not representative of the reservoir on the 100 m scale (permeability in the reservoir might be heterogeneous reflecting sedimentary layering); 3) the thickness measurements from the seismic reflection amplitudes are overestimates and a significant fraction of the injected CO_2 is not stored in the layers imaged, or 4) that model assumptions are inadequate. The volume of CO_2 imaged would need to be reduced to 19% of that injected for the whole-reservoir estimate of permeability to be compatible with the lower bound of measured permeabilities and the seismic data suggests this is unrealistic.

Important model approximations include ignoring capillary forces on the two phase brine-CO_2 interface, ignoring the variation in relative permeability with CO_2 saturation, and ignoring the viscous flow of the saline brine. Recent modelling of injection of less viscous fluids into formations initially filled with a more viscous fluid, shows the development of thinner, but larger radius accumulations [21]. Experiments are in progress for which the intruding fluid is of different viscosity to that in the ambient (Thompson and Huppert, to be submitted). When the dynamic viscosity of the current exceeded that of the ambient, a sharp boundary was observed between the two liquids. The boundary propagated at a rate which was well predicted by a theoretical approach similar to that used by Lyle et al. [11]. Experiments conducted with an intruding liquid whose dynamic viscosity was less than that of the ambient displayed a fuzzy boundary between the two liquids, characteristic of Saffman–Taylor fingering in a porous medium [22]. The propagation speed in this situation is, at least at the moment, not well predicted by the theoretical model.

We consider that the most likely cause of the discrepancy in both the laboratory experiments and the modelling of the Sleipner CO_2 layers arises from the reduction in relative permeability from two-phase flow. In particular, the outer parts of the spreading layers with low CO_2 saturations may have low permeabilities for the CO_2 phase. The calculated gas saturation at the displacement front from the Buckley–Leverett solution for analogous reservoir properties is ~0.3 and the gas relative permeability is ~0.03 [9,23]. Measurements on core samples from the Utsira Sand indicate that relative

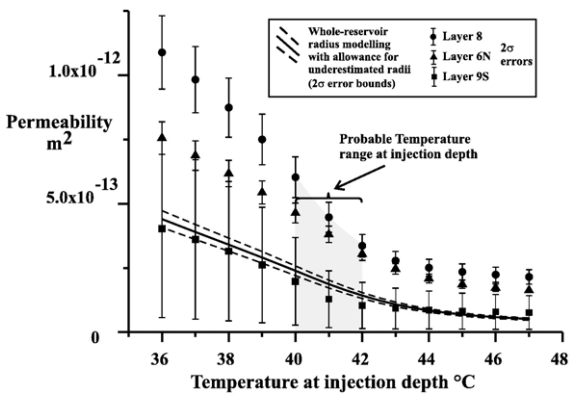

Fig. 10. Estimated permeabilities from whole-reservoir model and thickness-radius data from layers 6N, 8 and 9S as a function of temperature at injection depth. 2σ error bars reflect only uncertainties in least-squares fits to radius and thickness-radius data (Figs. 4 and 8). Most probable temperature at injection depth is 41 ± 1 °C.

permeabilities are <0.1 for CO_2 saturations <0.4 (Lindberg, personal communication, 2005). Such reductions would give permeabilities within the range estimated here and raises interesting questions about the state of CO_2 saturation within the CO_2 layers.

5. Conclusions

A theoretical model for flow of axisymmetric density fluids in a porous media [11] is used to analyse growing accumulations of CO_2 imaged by seismic reflection surveys at the Sleipner field in the North Sea. The accumulations exhibit the expected linear increase in their radius with square-root of time. The radius-squared versus time plots indicate that layers higher in the reservoir started accumulating substantially later than the start of injection of CO_2 in the field. Modelling of the time variation of thickness in two of these higher layers (6 North and 8) indicates that their CO_2 input increased with time. Conversely the lower layers indicate decreasing net CO_2 inputs with time. It seems most probable that lower layers progressively leaked more CO_2 through their thin cap-rock mudstones with time and the growth of the overlying layers reflects this increasing supply of CO_2 from below. Reservoir permeabilities estimated from the shape of the accumulations are below the range of measured values and it is not yet clear to what extent this discrepancy is a result of limitations in the modelling, a difference between permeability on the scale of the reservoir and the scale of the measurements or whether less CO_2 is stored in the layers imaged than estimated from the seismic studies. We consider that the most probable cause of the discrepancy is that the relative permeability for the CO_2 phase is significantly reduced at lower CO_2 saturations which raises questions concerning the CO_2 saturation within the accumulations.

The seismic reflection data, although providing good constraints on the development of the accumulations in plan view, is still subject to significant uncertainties in interpretation of accumulation thicknesses. If both radial and vertical dimensions were well constrained, modelling growth of the accumulations would provide important constraints both on reservoir properties (principally permeabilities on the scale of the accumulations), local flow rates and time dependent behaviour of the thin mudstone layers. The most useful aspect of the analytical modelling described here lies in its potential ability to predict likely plume volumes from the areal extents without the need for a full reservoir simulation. This would be particularly useful at the storage site selection stage where the technique would allow rapid assessment of different injection scenarios incorporating a wide range of reservoir parameters and uncertainties. The linear radius-squared to time relationship for accumulation growth means that the spreading layers would be most economically imaged by seismic surveys that repeat at constant intervals of the square-root of time. More frequent surveys early in the evolution of reservoirs would be valuable for modelling their subsequent evolution.

Acknowledgements

Jan Nordbotten kindly made available unpublished work. We thank the SACS and CO2STORE consortia for permission to publish this work and also the operators of the Sleipner license, Statoil, ExxonMobil, Norsk Hydro and Total for their co-operation. Andy Chadwick publishes with permission of the Executive Director, British Geological Survey (NERC). SACS and CO2STORE are funded by the EU Thermie Programme, by industry partners Statoil, BP, ExxonMobil, Norsk Hydro, Total and Vattenfall, and by national governments including the UK DTI. R and D partners are BGR, BGS, BRGM, GEUS, IFP, TNO-NITG, Schlumberger and SINTEF Petroleum Research. Research at BGS and Cambridge is funded by the NERC UKCCSC consortium. Research by HEH is supported by a Royal Society Wolfson Research Merit Award.

References

[1] H.J. Herzog, The economics of CO_2 capture, in: P. Riemer, B. Eliasson, A. Wokaun (Eds.), Greenhouse Gas Control Technologies, Elsevier Science Ltd., Amsterdam, 1999, pp. 101–106.

[2] E. Lindeberg, The quality of a CO_2 repository: what is the sufficient retention time of CO_2 stored underground? in: J. Gale, Y. Kaya (Eds.), Greenhouse Gas Control Technologies, vol. 1, Elsevier Science Ltd., Amsterdam, 2003, pp. 255–266.

[3] L.G.H. Van der Meer, R.J. Arts, L. Peterson, Prediction of migration of CO_2 injected into a saline aquifer: reservoir history matching to a 4D seismic image with a compositional gas/water model, in: D.J. Williams, R.A. Durie, P. McMullan, C. A.J. Paulson, A.Y. Smith (Eds.), Greenhouse Gas Control Technologies, CSIRO Publishing, Collingwood, 2000, pp. 378–384.

[4] H.E. Huppert, Geological fluid mechanics, in: G.K. Batchelor, H.K. Moffat, M.G. Worster (Eds.), Perspectives in Fluid Dynamics: A Collective Introduction to Current Research, Cambridge University Press, Cambridge, 2000, pp. 447–506.

[5] J. Rutqvist, C.-F. Tsang, A study of caprock hydromechanical changes associated with CO_2-injection into a brine formation, Environ. Geol. 42 (2002) 296–305.

[6] J.W. Johnson, J.J. Nitao, C.I. Steefel, K.G. Knauss, Reactive transport modelling of geologic CO_2 sequestration in saline aquifers: the influence of intra-aquifer shales and the relative effectiveness of structural, solubility, and mineral trapping during prograde and retrograde sequestration, First National Conference

on Carbon Sequestration, National Energy Technology Laboratory, Washington, DC, 2001.
[7] K. Pruess, J. Garcia, Multiphase flow dynamics during CO_2 disposal into saline aquifers, Environ. Geol. 42 (2002) 282–295.
[8] E. Lindeberg, P. Zweigel, P. Bergmo, A. Ghaderi, A. Lothe, Prediction of CO_2 distribution pattern by geology and reservoir simulation and verified by time lapse seismic, in: D. Williams, R. Durie, P. McMullan, C. Paulson, A. Smith (Eds.), Greenhouse Gas Control Technologies, CSIRO Publishing, Collingwood, 2003, pp. 372–377.
[9] K. Pruess, T. Xu, J. Apps, J. Garcia, Numerical modeling of aquifer disposal of CO_2, SPE J. 8 (2003) 49–60.
[10] H.E. Huppert, A.W. Woods, Gravity flows in porous layers, J. Fluid Mech. 292 (1995) 55–69.
[11] S. Lyle, H.E. Huppert, M. Hallworth, M. Bickle, A. Chadwick, Axisymmetric gravity currents in a porous medium, J. Fluid Mech. 543 (2005) 293–302.
[12] R. Arts, O. Eiken, A. Chadwick, P. Zweigel, L. Van der Meer, B. Zinszner, Monitoring of CO_2 injected at Sleipner using time-lapse seismic data, Energy 29 (2004) 1383–1392.
[13] R.A. Chadwick, R. Arts, O. Eiken, G.A. Kirby, E. Lindberg, P. Zweigel, 4D seismic imaging of an injected CO_2 plume at the Sleipner Field, central North Sea, in: R.J. Davies, J.A. Cartwright, S.A. Stewart, M. Lappin, J.R. Underhill (Eds.), 3D Seismic Technology: Application to the Exploration of Sedimentary Basins, Geological Society, London, Memoires, vol. 29, Geological Society of London, Bath, 2004, pp. 311–320.
[14] P. Zweigel, P. Arts, A.E. Lothe, E. Lindeberg, Reservoir geology of the Utsira Formation at the first industrial-scale under-ground CO_2 storage site (Sleipner area, North Sea), in: S. Baines, R. Worden (Eds.), Geological Storage for CO_2 Emissions Reductions, Geological Society of London, Special Publications, vol. 233, Geological Society of London, 2004, pp. 165–180.
[15] R.A. Chadwick, R. Arts, O. Eiken, 4D seismic quantification of a growing CO_2 plume at Sleipner, North Sea, in: A.G. Dore, B.A. Vining (Eds.), 6th Petroleum Geology Conference, Geological Society London, vol. 6, Geological Society London, 2005, pp. 1385–1399.
[16] D. Vella, H. Huppert, Gravity currents in a porous medium at an inclined plane, J. Fluid. Mech. 555 (2006) 353–362.
[17] S. Lyle, Interpretation of time-lapse seismic data from the CO_2 storage operation at Sleipner, northern North Sea, MSci Thesis, University of Cambridge, (2005).
[18] J. Kent, G. Watson, T. On Stott, Fitting straight lines and planes with an application to radiometric dating, Earth Planet. Sci. Lett. 97 (1990) 1–17.
[19] K. Pruess, The TOUGH codes — a family of simulation tools for multiphase flow and transport processes in permeable media, Vadose Zone Journal 3 (2004) 738–746.
[20] P. Zweigel, A. Lothe, R. Arts, M. Hamburg, Reservoir geology of the storage units in the Sleipner CO_2-injection case. A contribution to the saline aquifer CO_2 storage project (SACS), SINTEF Petroleum Research Report Confidential, (2000) 23.4285.00/02/00, 79 pp.
[21] J.R. Nordbotten, M.A. Celia, Similarity solutions for fluid injection into confined aquifers, J. Fluid Mech. 561 (2006) 307–327.
[22] G.M. Homsy, Viscous fingering in porous-media, Annu. Rev. Fluid Mech. 19 (1987) 271–311.
[23] C. Doughty, K. Pruess, Modeling supercritical carbon dioxide injection in heterogeneous porous media, Vadose Zone Journal 3 (2004) 837–847.